coatings

Article

Adhesion Strength and Anti-Corrosion Performance of Ceramic Coating on Laser-Textured Aluminum Alloy

Changfeng Fan [1,2], Xue Wang [3,*], Xiaoli Yin [1], Wei Huang [1,4], Yujie Da [1], Hao Jiang [1], Jingfeng Cao [1], Yongchao Gai [1] and Wangwang Zhang [5]

1 College of Intelligent Manufacturing and Control Engineering, Shandong Institute of Petroleum and Chemical Technology, Shandong 257061, China; fancf2015@hotmail.com (C.F.); yinxl@sdipct.edu.cn (X.Y.); hwei18231303568@163.com (W.H.); dayujie0731@163.com (Y.D.); 17661250686@163.com (H.J.); y18853008092@163.com (J.C.); gaiyongchao2025@163.com (Y.G.)
2 Key Laboratory of Mechanical Surface Engineering and Tribology, Shandong Institute of Petroleum and Chemical Technology, Shandong 257061, China
3 College of Chemical Engineering, China University of Petroleum, Shandong 266580, China
4 Dongying Pinmo Import and Export Co., Ltd., Shandong 257061, China
5 Dongying City Infrastructure Pipeline Natural Gas Limited Liability Company, Shandong 257061, China; shilong19891225@126.com
* Correspondence: xuewang0822@163.com

Abstract: Laser surface texturing and micro-arc oxidation provide excellent approaches to enhance the adhesion strength and anti-corrosion performance of adhesive bonding interfaces in aluminum alloys, which can be applied in the field of automotive light weighting. Herein, micro-arc oxidation coatings were fabricated on the laser-textured aluminum surface under the voltage of 500 V for various treatment times (5 min, 15 min, 30 min, 60 min). The anti-corrosion performance of ceramic coatings on the laser-textured surface was analyzed using electrochemical measurements. The results of electrochemical measurement indicate that the coating on the sample surface presents two time constants corresponding to a dual-layer structure. The sample grown under 500 V for 60 min exhibits excellent protective performance with a value of 1.3×10^7 ohm·cm^2. The adhesion strength of laser-textured ceramic coating is improved compared with the as-received substrate. The sample treated with 500 V for 30 min exhibits the highest bonding strength with a value of 52 MPa. The wider pores and bulges for the sample grown in 60 min would introduce microcracks and consequently reduce the adhesion strength.

Keywords: micro-arc oxidation; laser texture; aluminum alloy; electrochemical measurement; adhesive bonding

check for updates

Citation: Fan, C.; Wang, X.; Yin, X.; Huang, W.; Da, Y.; Jiang, H.; Cao, J.; Gai, Y.; Zhang, W. Adhesion Strength and Anti-Corrosion Performance of Ceramic Coating on Laser-Textured Aluminum Alloy. *Coatings* **2023**, *13*, 2098. https://doi.org/10.3390/coatings13122098

Academic Editor: Avik Samanta

Received: 21 November 2023
Revised: 12 December 2023
Accepted: 13 December 2023
Published: 17 December 2023

1. Introduction

Aluminum alloy, known for its exceptional combination of low density and high strength, has become an essential material in various industries, such as automotive [1] and aerospace industries [2]. The application in lightweight structural components effectively enhances performance [3,4]. Their light weight contributes to fuel economy, reducing the overall weight of the vehicle without compromising the structural integrity in the automotive industry, while the aerospace industry relies on aluminum alloys for their structural components, due to their strength-to-weight ratio, corrosion resistance, and compatibility with manufacturing processes. However, aluminum alloys present specific weldability challenges, especially when joining dissimilar materials. Adhesive bonding, an efficient, cost-effective, and environmentally friendly processing technique, has emerged as an alternative. It not only reduces the structural weight by about 25%–30% compared to traditional methods like riveting and welding, but also provides advantages including decreased stress concentrations at joints, corrosion resistance, and efficiency [5,6].

The surface modification of aluminum plays a central role in determining adhesion strength and durability for applications. Laser texturing has attracted much attention by creating diverse micro- and nanostructures with many advantages [7]. F. Lambiase et al. treated aluminum surfaces before joining to enhance the mechanical interlock between substrates by laser texturing [8]. Wan et al. demonstrated that laser treatment induces physicochemical changes, increasing joint strength by 374% and transitioning the failure mode from interfacial to mixed [9]. However, adhesive joints encountered the degradation and poor durability stemming from the interfacial corrosion in humid, hot environments. In light of this, Bora et al. investigated laser texturing and silane treatment on adhesive performance [10]. Notably, silane treatment's effect on interfacial bond strength is unpredictable and may reduce interfacial bond strength.

Micro-arc oxidation (MAO) is considered an eco-friendly and effective surface treatment for aluminum. MAO exploits transient high-temperature and high-pressure conditions created by an electrical discharge in an electrolyte solution to promote in situ generation of oxide ceramic films on metal surfaces, including magnesium, aluminum, and titanium. The electrical parameters have a significant impact on the discharge energy, ultimately influencing the microstructure of the ceramic coating. Wang et al. emphasized that coatings with remarkable corrosion resistance can be obtained by controlling process parameters [11]. Many studies have explored the corrosion resistance of MAO-treated aluminum surfaces, confirming its effectiveness. The corrosion resistance performance is closely associated with process parameters and electrolyte composition. Tran et al. achieved rapid growth of the micro-arc oxidation layer and improved corrosion resistance and hardness by adding ammonia to the sodium silicate electrolyte solution [12], while Wang et al. adjusted the electrical parameters to obtain a coating with improved corrosion resistance [13]. The dense ceramic coatings exhibit excellent corrosion properties [14–16]. Furthermore, Guan et al. involved the MAO treatment of valve metal surfaces, resulting in significant adhesive property improvements [17]. The mechanical bond strength is further improved as the coating roughness and micropore size on the surface increase. Physical interlocking of the ceramic coating and substrate contributes to excellent adhesion [18–21]. These ceramic coatings exhibit high bonding strength and other advantages such as excellent durability, corrosion resistance, and insulation. Micro-arc oxidation application has the potential to significantly improve the surface strength and corrosion resistance of aluminum alloys [22–24]. However, less attention has been paid to correlations between laser surface texturing and MAO on the adhesion strength of the 5052 aluminum alloy.

In this work, 20 W nanosecond pulsed laser pulses were used to fabricate microholes in the 5052 aluminum alloy substrate. We investigated the impact of micro-arc oxidation treatment time on the corrosion resistance and adhesion strength performance of the laser-textured surface. The aim was to evaluate the performance of the combination of laser surface texturing and micro-arc oxidation on adhesion strength. The influence of micro-arc oxidation time on the adhesion strength of laser microtextured surfaces will be elucidated. Other parameters, such as the electrolyte, voltage, and current density, will not be discussed in this study. The micromorphology of ceramic coatings was characterized by scanning electron microscopy (SEM) and analyzed using an energy-dispersive spectrometer (EDS). The corrosion resistance was evaluated on an electrochemical workstation. The adhesion strength was measured by the pull-out method.

The objective is to determine the optimal parameters for the micro-arc oxidation application of aluminum alloys, providing both theoretical information and technical support for the advancement of lightweight materials in the automotive industry. The combination of increased strength and suitable surface properties can lead to the development of lightweight components with improved durability and corrosion resistance. The study not only contributes to ongoing efforts in materials science for automotive applications but also highlights the importance of surface engineering techniques in pushing the limits of performance and functionality of lightweight materials.

2. Materials and Methods

2.1. Material and Coating Preparation

The chemical compositions of the 5052 aluminum alloy used in this research are shown in Table 1. Plates with a thickness of 2 mm were cut to dimensions of 25 mm × 50 mm.

Table 1. Chemical composition of 5052 aluminum alloy (in wt%).

Element	Si	Fe	Cu	Mn	Mg	Cr	Zn	Al
Content	0.06	0.21	0.01	0.01	2.66	0.19	0.01	Bal.

The samples were polished using sandpaper until they reached a grit of #2400, after which they were dipped into a 4 g/L NaOH solution at 80 °C for 10 min. Afterwards, the samples were soaked in a 10% HCl solution at room temperature for 2 min and subsequently washed with deionized water.

2.2. Laser Surface Texturing and Micro-Arc Oxidation Treatment

The nanosecond laser system (KX-200) is represented in Figure 1 with a schematic illustration. Samples were mounted on a 3-dimensional translation stage. A 20 W pulsed laser was used to generate a sinusoidal pattern on aluminum, as shown in Figure 1. The scanning speed was set at 1000 mm/s. This study aims to investigate and improve adhesion strength through combined laser microtexturing and micro-arc oxidation. The distinction in bonding strength is also influenced by laser texturing parameters. Further information is essential to elucidate this point.

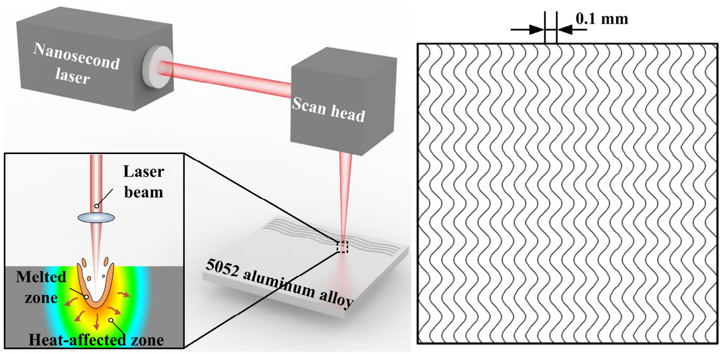

Figure 1. Schematic illustration of the nanosecond laser system.

A series of samples was obtained by micro-arc oxidation using the experimental system shown in Figure 2. The silicate electrolyte with KOH (4 g/L) and K_2TiF_6 (5 g/L) was introduced. Micro-arc oxidation was conducted at 750 Hz, with a positive-to-negative duty ratio of 35% and a current density of 2 A/dm^2. The laser-textured substrate was treated with various treatment times, as shown in Table 2. The voltage was selected as 500 V for micro-arc oxidation. To remove residual alkali solution on the ceramic coating surface and prevent erosion, the fabricated samples were immersed into deionized water with 5–10 min ultrasonication treatment and then dried.

Table 2. The treatment method and treatment time utilized in this study.

No.	Surface Treatment	MAO Voltage (V)	MAO Time (min)
1	As-received	-	-
2	LST	-	-
3	LST + MAO	500	30
4	LST + MAO	500	5
5	LST + MAO	500	15
6	LST + MAO	60	60

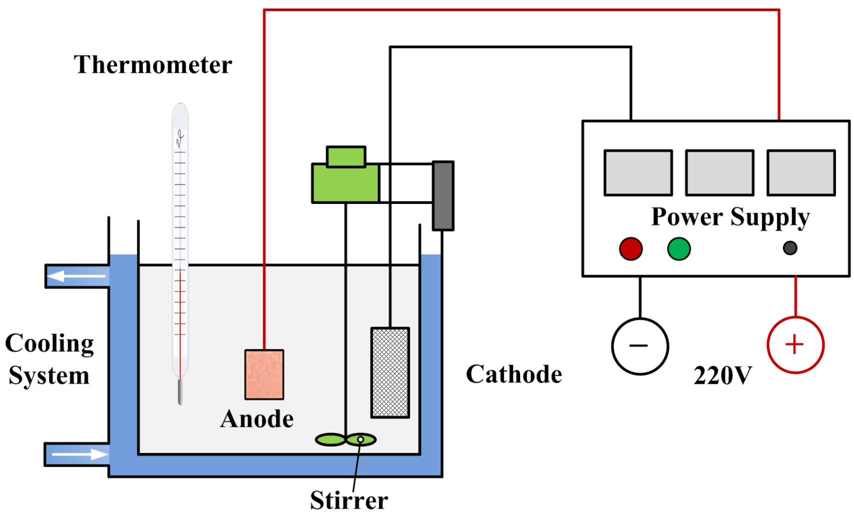

Figure 2. The micro-arc oxidation experimental system.

2.3. Characterization Methods and Electrochemical Measurement

MAO ceramic coatings were observed via scanning electron microscope (SEM, SUS3800, Hitachi, Tokyo, Japan). The texture geometry was evaluated by the 3D profile measurement microscope (VHX-5000, KEYENCE, Osaka, Japan). Energy-dispersive X-ray spectroscopy (EDS) characterized element distribution and content on the ceramic coatings.

Electrochemical measurements were carried out by an electrochemical workstation with a 3.5 wt% NaCl solution (Reference 3000, Gamry, Warminster, PA, USA). A three-electrode system was employed with the sample as the working electrode. A platinum mesh was regarded as the counter electrode. The reference electrode was selected as an Ag/AgCl electrode (3M KCl). Potentiodynamic (DP) measurements were conducted with the scanning rate of 1 mV/s (over ±0.1 V vs. open circuit potential). Electrochemical impedance spectroscopy was performed with the following characteristics: exposure area of 1 cm^2, frequency from 100 kHz to 0.01 Hz with the voltage amplitude of 20 mV. Acquired data were analyzed using Zview software (Version 3.2) with specified equivalent circuit models to obtain comprehensive information on the electrochemical behavior of the measured samples.

2.4. Characterization Methods and Electrochemical Measurement

The epoxy (AV138M-1, ARALDITE, Basel, Switzerland) was selected as the adhesive in this study. The base and hardener of the two-component coating were completely blended together. The coating was placed in a ventilated environment at 25 °C for seven days to carry out the follow-up test. The adhesion strength for the interface was evaluated based on the ASTM D4541-2017 standard test method [25].

3. Results and Discussion

The ablation signature indicates sequential layer-by-layer removal of material, similar to the ablation observed in Al_2O_3 when fabricated with a picosecond laser [26]. As depicted in Figure 3a, a distinct microwall-like structure is formed due to the melted and recast material. This phenomenon is further emphasized by the inward flow of the molten material stemming from the impact of laser pulses. The presence of the microwall structure above the aluminum substrate increases the depth, which is positive to the enhancement of adhesion strength.

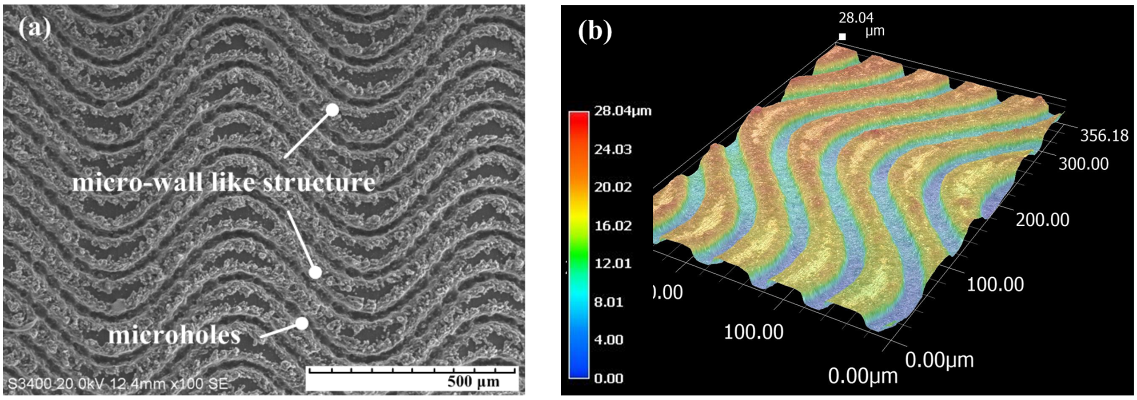

Figure 3. SEM top-view of laser texture (**a**) and 3D profile microscope images (**b**) of aluminum surface.

Figure 3b indicates the 3D profile microscope images of the aluminum surface with the microtexture. Microvalleys with complex structures were fabricated by nanosecond laser ablation, reaching a vertical depth of approximately 28 µm. During nanosecond laser ablation of the aluminum surface to create lines, many nanoparticles and microparticles were removed and then deposited along the sides of the ablated lines. These particles were redeposited along two sides of the ablated lines. The depth illustrates nonuniformity. Rims and valleys can be observed. This inhomogeneity arises from the formation and expulsion of molten material owing to local high pressure during laser texturing. The formation of recast material both within and around the concealed microholes contributes to the growth of microwalls surrounding blind micropores.

The SEM surface morphology of the ceramic layers on the laser-textured aluminum surface grown at 500 V for 30 min is depicted in Figure 4. A porous structure is observed. The sample develops an in situ MAO ceramic coating on the laser-textured substrate. The aluminum surface has a microtextured structure with ridges and valleys (Figure 4b) in addition to micro-nanoholes in the micro-arc oxidation coating. It is worth emphasizing that applying high voltage causes electrical sparks stemming from a higher electrical current. The strong electric avalanches lead to the initiation of wider micropores. When the voltage applied is high, the positive voltage more easily suffers from the breakdown potential of the ceramic coating. Consequently, lots of electron avalanches occur in the vicinity of the anode leading to more pore initiation. The consolidation of the structural pores is a result of the high-energy sparks [27]. The ceramic coating is subjected to high electric current in order to sinter it. The laser-textured aluminum substrate has more concave and convex microstructuring than the as-received aluminum alloy with faster molten oxidation in protruding parts. The bonding strength would be affected. According to the EDS mapping results shown in Figure 5, element mapping of Al, O, Si, Mg, and Ti indicates that these elements are homogeneously distributed in the coating. The surface analysis results from the EDS are presented in Table 3, giving an indication of the proportion for each element. The analysis showed that Al and O were found in the film, occupying a large proportion, whereas Si, Mg, and Ti account for relatively smaller proportions. The ceramic coating is mostly composed of silicon–oxygen, magnesium–oxygen, and titanium–oxygen compounds. Silicon–oxygen compounds have an influence on the roughness of the MAO coating. The presence of titanium–oxygen compounds can positively enhance the corrosion properties.

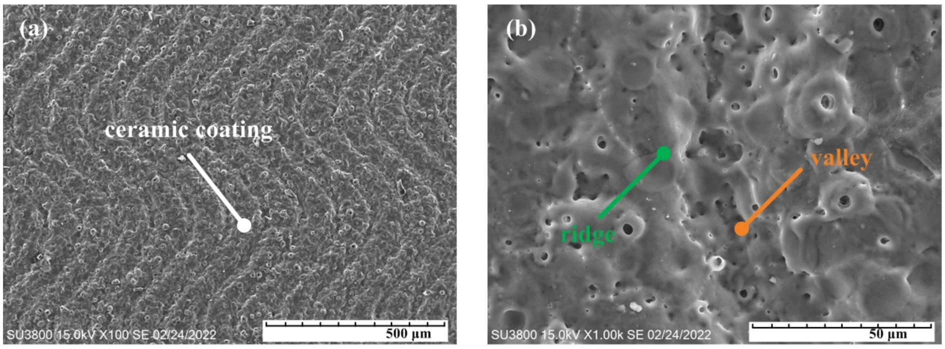

Figure 4. SEM top-view of the MAO coatings on laser-textured aluminum substrate grown at 500 V for 30 min. (**a**) 100×. (**b**) 1000×.

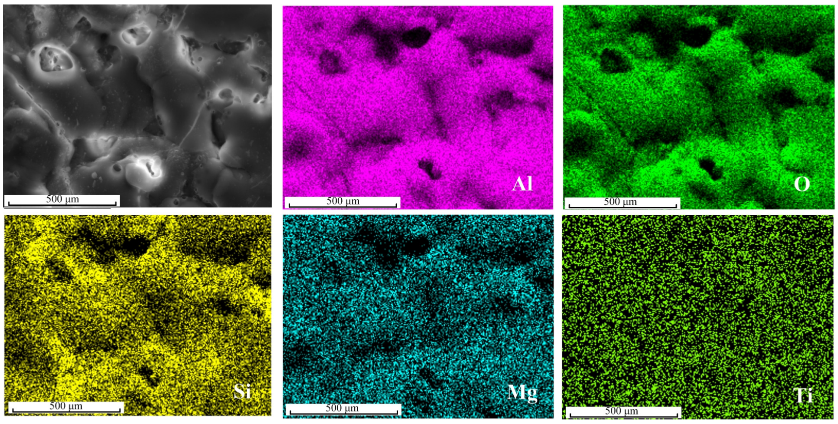

Figure 5. EDS elemental mapping of laser-textured aluminum with MAO treatment at 500 V for 30 min.

Table 3. The compositions on surfaces from EDS analysis (wt%).

Elements	Al	O	Si	Mg	Ti
content	43.79	41.20	5.81	4.51	3.75

The coating that was developed at a voltage of 500 V displayed a suitable morphology and chemical composition. Herein, the textured samples were fabricated by micro-arc oxidation at 500 V for 5 min, 15 min, and 60 min. It is worth reminding that the growth time of 30 min was investigated earlier. Figure 6 illustrates the impact of growth time on the surface morphology of the coatings. It can be observed that the diameter of pores increases over the treatment time, whereas there are cracks and breakdowns on the coarse surface [28]. The diameter of the micropore is appropriately 3 µm for the ceramic coating grown under the condition of 500 V for 30 min. The formation of a structural pore through an electrical spark increases its susceptibility to subsequent electron avalanches due to its lower breakdown voltage compared to non-porous areas. Furthermore, the sequential occurrence of electrical sparks at a single point leads to larger pores. The coating became exfoliative and coarse when the applied voltage exceeded a critical value for an extended treatment time, making optimization impossible to a certain extent. Jiang et al. demonstrated that high voltage in the electrolyte led to the occurrence of intense sparking arcs, resulting in negative consequences like the thermal cracking of coatings [29]. A lot of bulges can generate under the condition of 500 V for 60 min. The formation of wider pores and bulges initiates microcracks, which in turn reduce the surface area and subsequently weaken the adhesion between the coating and the substrate.

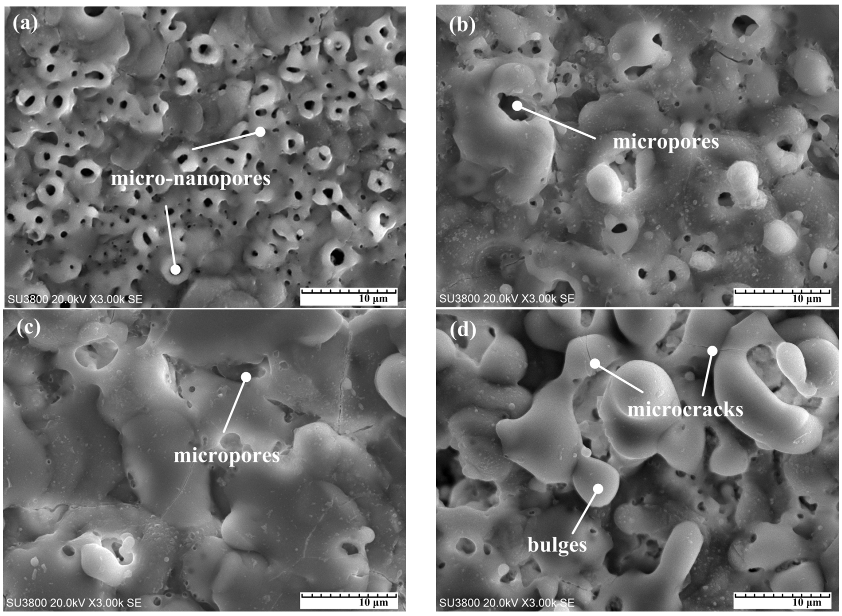

Figure 6. SEM top-view of the micro-arc oxidation coatings grown under the voltage of 500 V for different times: (**a**) 5 min, (**b**) 15 min, (**c**) 30 min, (**d**) 60 min.

The potentiodynamic polarization curves of the coatings are illustrated in Figure 7. The results show that the corrosion potential of ceramic coatings is almost similar to that on the substrate. However, the MAO coating exhibits a relatively lower current density, which can be related to the presence of metal oxides in the coatings. Based on Figure 7a, it can be observed that the coatings display a consistent decrease in corrosion current density as the voltages increase, while corrosion potential and polarization resistance continuously increase. A low corrosion current density suggests a good corrosion resistance. The corrosion potential and polarization resistance of the bare substrate are −680 mV and 0.69 µA/cm^2, respectively. These values slightly increase to −650 mV and 0.63 µA/cm^2 for the laser-textured surface. The ceramic coating after LST exhibits a maximum of −616 mV and 4.47 nA/cm^2, respectively. The current density dropped almost two orders of magnitude compared to that of the substrate. Figure 7b illustrates the potentiodynamic polarization curves of ceramic coatings obtained under 500 V with different treatment time. The corrosion current density noticeably decreases as the treatment time increases, reaching a minimum of 2.04 nA/cm^2 after 60 min. The current density of the MAO sample was more than 100 times lower than that of the substrate.

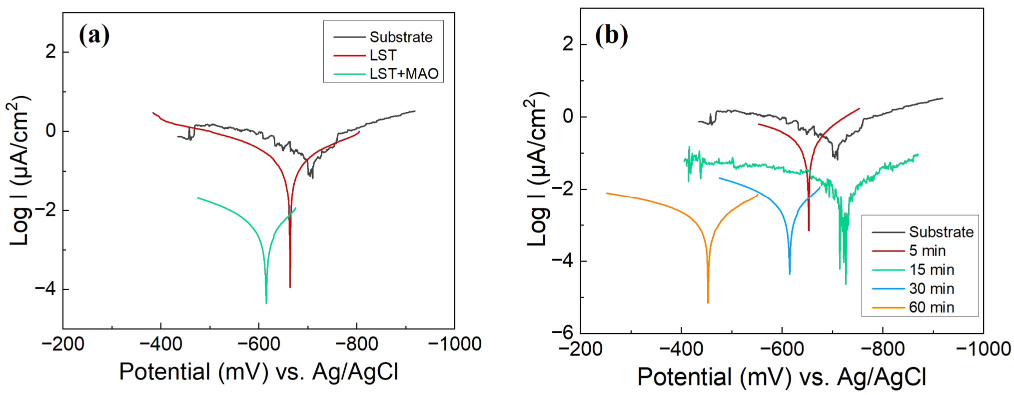

Figure 7. Polarization curve for (**a**) different surface treatment on 5052 aluminum alloy and (**b**) different MAO treatment time at 500 V.

Figure 8a illustrates impedance spectra in the Nyquist plot for the aluminum substrate with/without laser texturing and micro-arc oxidation. Generally, the relationship between resistance and capacitance in charge transfer processes can be reflected by the impedance arc in the Nyquist plots. The radius of the arc on the impedance is directly proportional to the corrosion resistance of the sample. A larger radius indicates better corrosion resistance [30–32]. The Nyquist plots of the substrate with/without laser texturing indicate similar electrochemical behavior. Poor corrosion resistance can be observed in the substrate for 1.04×10^5 ohm·cm^2. However, micro-arc oxidation coating can effectively enhance the impedance. Laser microtexturing mainly affects the microscopic surface morphology of the substrate, while micro-arc oxidation leads to the formation of a ceramic coating between the substrate and electrolyte, showing the possibility of excellent corrosion resistance. The Nyquist plot shows its high impedance characteristics. The complex plane of coating grown on the textured surface at 500 V for 30 min was manifested as a straight line, which exhibits the highest impedance with about 2×10^6 ohm·cm^2.

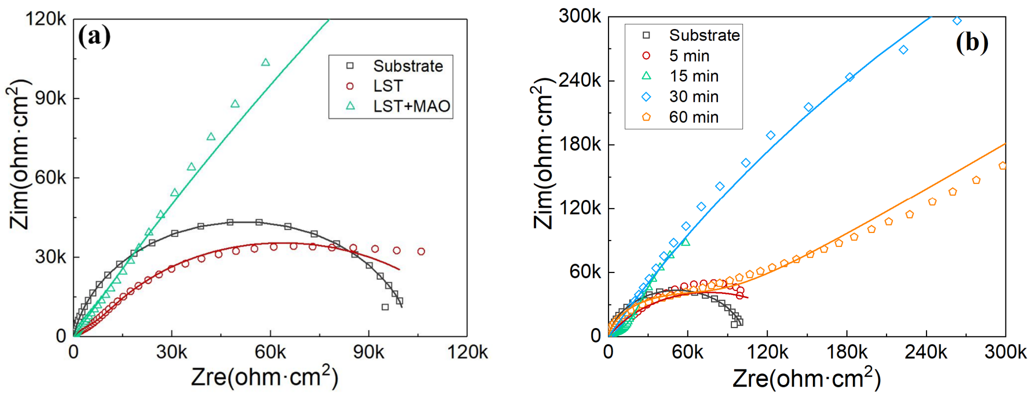

Figure 8. EIS spectra for (**a**) different surface treatment on 5052 aluminum alloy and (**b**) different MAO treatment time at 500 V.

Figure 8b shows the Nyquist and Bode plots of micro-arc oxidation coatings grown under different treatment times. The Nyquist plot of the sample grown under 500 V for 60 min displays a large arc that does not end in the low-frequency range, which indicates the excellent protective performance. The compressed arc, implying two overlapping time constants, can be deduced from the Nyquist plots for all samples. As the micro-arc oxidation time increases, the thickness of the ceramic coating continues to increase, thus leading to a corresponding increase in its impedance. The values of the impedance modulus increased remarkably from 1.16×10^5 ohm·cm^2 to more than 10^7 ohm·cm^2. The sample grown at 500 V for 60 min displays a very high impedance with a value of 1.3×10^7 ohm·cm^2.

Figure 9 illustrates the equivalent circuit to elucidate the EIS spectra for the samples with and without micro-arc oxidized coatings. Model A and model B are employed to fit the EIS spectra of the substrate and textured sample with ceramic coating, respectively. Constant phase elements (CPEs) are incorporated into the equivalent circuit. R_e represents the electrolyte resistance. R_1 and CPE_1 indicate the equivalent resistance and capacitance of the outer layer of the coating, while R_2 and CPE_2 represent the equivalent resistance and capacitance of the inner layer of the coating. Generally, the condensed inner layer exhibits better corrosion resistance for external corrosive ions, resulting in higher impedance values. Conversely, the micro-arc oxidation outer layer of the coating is thinner and contains certain voids, facilitating the passage of corrosive ions and thus leading to a relatively lower impedance value. Polarization resistance R_{pl} ($R_{pl} = R_1 + R_2$) is commonly considered as a parameter to evaluate the protective performance. The sample fabricated under the condition of 500 V for 60 min exhibits the highest resistance value of 1.3×10^7 ohm·cm^2, indicating the best corrosion resistance among the samples. This suggests that this is an appropriate voltage to reduce the number and size of pores. Moreover, the formed oxides such as Al_2O_3 and TiO_2 can obstruct the erosion of corrosive ions, enhancing the corrosion resistance of the ceramic coating [33,34].

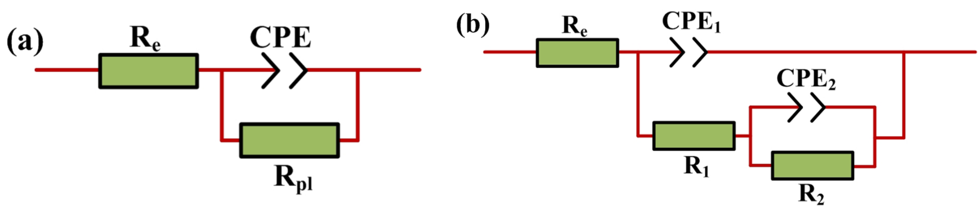

Figure 9. Equivalent circuit diagrams of EIS for aluminum alloy with various surface treatments and MAO treatment times. (**a**) Model A. (**b**) Model B.

Sandblasting is widely regarded as a method of surface treatment, but noise and dust from sandblasting may be detrimental to the environment. Furthermore, as indicated in Table 4, preliminary experimental studies show slightly lower adhesion strength in the samples with sandblasting + MAO treatment compared to those treated with LST + MAO. The combination of laser microtexturing and micro-arc oxidation can create a structure on the substrate similar to a gecko's foot pad, which can increase adhesion strength. The laser microtexturing treatment is at the center of our attention here. The tensile test results of the substrate with and without laser texture and micro-arc oxidation are revealed in Figure 10. Compared with the bare substrate, the textured sample shows an adhesion strength improvement of 65% with 33 MPa. The textured sample with micro-arc oxidation illustrates improved adhesion strength with the value of 52 MPa. According to the SEM graphs, it is clear that in samples without MAO treatment, the adhesive components are damaged at the interface between the adhesive layer and the substrate. In contrast, for samples subjected to MAO treatment, the adhesive layer exhibited fractures, resulting in cohesive failure. This result can be relevant to the porous surface of the aluminum. The presence of pores on the surface would promote a mechanical interlock between the oxide layer and the adhesive. When the ceramic coating is subjected to tensile loading, the distribution and configuration of pores in fact lead to weaknesses in the bonds [35]. The textured aluminum treated with micro-arc oxidation exhibits enhanced adhesive strength from 33 MPa to the maximum of 52 MPa. Laser texturing effectively minimizes both breakage and delamination of MAO coatings, consequently reducing the formation of the peeling layer. This is achieved by forming an oxide layer after undergoing micro-arc oxidation treatment. It can be observed that the textured sample with/without micro-arc oxidation exhibits a similar fractured morphology characterized by an identical pattern. However, it is important to note that the sample without ceramic coating presents adhesive failure, while the textured sample with micro-arc oxidation indicates cohesive fracture.

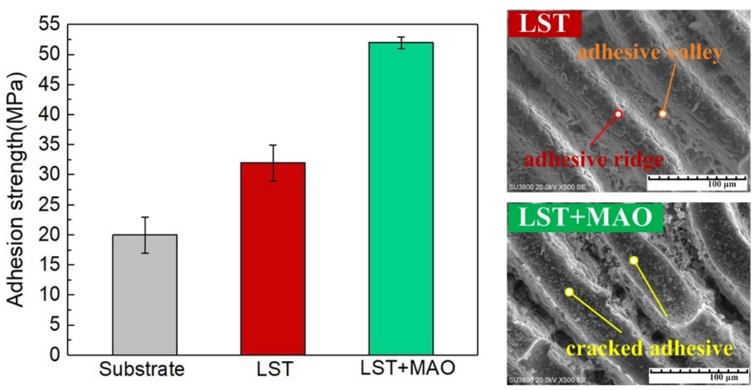

Figure 10. Adhesion strength of aluminum alloy under different surface treatments.

Table 4. The adhesion strength for different surface treatments.

Surface Treatment	Adhesion Strength (MPa)
As-received	20 ± 3
Sandblasting	30 ± 1.5
LST	33 ± 3
Sandblating + MAO	46 ± 1.5
LST + MAO	52 ± 1

Figure 11 illustrates the tensile test results of the ceramic coatings grown at 500 V with treatment times. The adhesion strength gradually increases during 5 to 30 min of micro-arc oxidation treatment. However, as the treatment time extends to 60 min, the adhesion strength decreases slightly to 45 MPa. It may be suggested that the presence of the oxide layer determined the bond strength of the aluminum–epoxy system. The findings of this research align with previous studies that attribute decreased bond strength to the presence of a thick oxide layer on the metal surface [36]. The wider pores and bulges for the sample grown in 60 min shown in Figure 6d would introduce the microcracks and consequently reduce the bonding strength between the coating and the substrate. Contrarily, Figure 6c revealed a compact and smooth structure with minimal large pores. This feature is advantageous as it enhances the effective contact area between the coating and the substrate while also preventing any potential breakage or spalling.

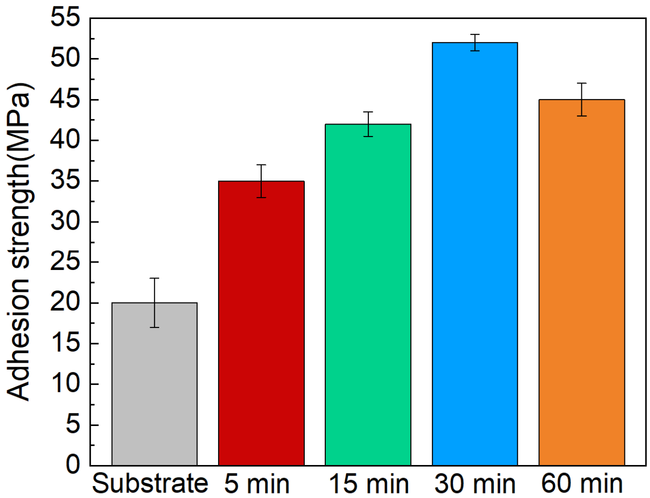

Figure 11. Adhesion strength of laser-textured aluminum alloy under different MAO treatment times.

4. Conclusions

This study investigated the influence of micro-arc oxidation treatment times on the adhesion strength and corrosion mechanism of ceramic coating on laser-textured 5052 aluminum alloy. The size of pores increases with the applied voltage because of the higher electrical current flowing through the electrochemical cell. The diameter of the micropore is appropriately 3 μm for the MAO coating grown under the condition of 500 V for 30 min. The Nyquist plot of the sample grown under 500 V for 60 min displays a large arc, which indicates an excellent protective performance with a value of 1.3×10^7 ohm·cm^2. The textured aluminum treated with micro-arc oxidation exhibits enhanced adhesive strength ranging from 33 MPa to 52 MPa. The sample without ceramic coating presents adhesive failure, while the textured sample with micro-arc oxidation indicates cohesive fracture. The sample treated with 500 V for 30 min exhibits the highest bonding strength. The wider pores and bulges for the sample grown in 60 min would introduce the microcracks and consequently reduce the bonding strength between the coating and the substrate. This study mainly focuses on the combined effects of laser microtexturing and micro-arc oxidation on the adhesion strength of the aluminum alloy surface. Several parameters play a role in this process, such as laser microtexture pattern, laser processing parameters, electrical parameters for micro-arc oxidation, and electrolyte composition. Further information is essential to explore and elucidate the influence of these factors.

Author Contributions: Conceptualization, C.F.; methodology, X.W. and X.Y.; investigation, W.H., Y.D. and H.J.; formal analysis, J.C.; data curation, Y.G.; writing—original draft preparation, C.F.; writing—review and editing, X.W., X.Y. and W.Z.; funding acquisition, C.F., X.W. and X.Y. All authors have read and agreed to the published version of the manuscript.

Funding: This work is supported by Dongying Science and Technology Development Foundation (DJ2020016, FZ20220027) and Shandong Provincial Natural Science Foundation (ZR2022QE186, ZR2021ME180, ZR2023QE139).

Institutional Review Board Statement: Not applicable.

Informed Consent Statement: Not applicable.

Data Availability Statement: The corresponding author can provide the data supporting the findings of this study upon reasonable request.

Conflicts of Interest: Author Wei Huang was employed by Dongying Pinmo Import and Export Limited Liability Company. Author Wangwang Zhang was employed by Dongying City Infrastructure Pipeline Natural Gas Limited Liability Company. The remaining authors declare that the research was conducted in the absence of any commercial or financial relationships that could be construed as a potential conflict of interest.

References

1. Jin, Q.H.; Chen, J.; Peng, L.M.; Li, Z.Y.; Yan, X.; Li, C.X.; Hou, C.C.; Yuan, M.Y. Research progress in joining of carbon fiber-reinforced polymer composites and aluminum/magnesium alloys. *J. Mater. Eng.* **2022**, *50*, 15–24.
2. Zhang, J.; Dai, W.; Wang, X.; Wang, Y.; Yue, H.; Li, Q.; Yang, X.; Guo, C.; Li, C. Micro-arc oxidation of Al Alloys: Mechanism, microstructure, surface properties, and fatigue damage behavior. *J. Mater. Res. Technol.* **2023**, *23*, 4307–4333. [CrossRef]
3. Wang, S.; Peng, X.; Yang, Y.; Wang, S.; Wu, M.; Hu, P.; Fu, C. Insight into microstructure evolution and corrosion mechanisms of K_2ZrF_6/Al_2O_3-doped hot-dip aluminum/micro-arc oxidation coatings. *Coatings* **2023**, *13*, 1543. [CrossRef]
4. Li, L.; Yang, E.; Yan, Z.; Xie, X.; Wei, W.; Li, W. Effect of pre-anodized film on micro-arc oxidation process of 6063 aluminum alloy. *Materials* **2022**, *15*, 5221. [CrossRef] [PubMed]
5. Budzik, M.K.; Wolfahrt, M.; Reis, P.; Kozłowski, M.; Sena-Cruz, J.; Papadakis, L.; Nasr Saleh, M.; Machalicka, K.V.; Teixeira de Freitas, S.; Vassilopoulos, A.P. Testing mechanical performance of adhesively bonded composite joints in engineering applications: An Overview. *J. Adhes.* **2021**, *98*, 2133–2209. [CrossRef]
6. Gong, W.; Ma, R.; Du, A.; Zhao, X.; Fan, Y. The effects of the pre-anodized film thickness on growth mechanism of plasma electrolytic oxidation coatings on the 1060 Al substrate. *Materials* **2023**, *16*, 5922. [CrossRef] [PubMed]
7. Zou, X.; Liu, L.; Chen, T.; Wu, L.; Chen, K.; Kong, L.; Wang, M. Laser surface treatment to enhance the adhesive bonding between steel and CFRP: Effect of laser spot overlapping and Pulse Fluence. *Opt. Laser Technol.* **2023**, *159*, 109002. [CrossRef]
8. Lambiase, F.; Yanala, P.B.; Leone, C.; Paoletti, A. Influence of laser texturing strategy on thermomechanical joining of AA7075 aluminum alloy and Peek. *Compos. Struct.* **2023**, *315*, 116974. [CrossRef]
9. Wan, H.; Min, J.; Lin, J. Experimental and theoretical studies on laser treatment strategies for improving shear bonding strength of structural adhesive joints with cast aluminum. *Compos. Struct.* **2022**, *279*, 114831. [CrossRef]
10. Bora, M.; Çoban, O.; Akman, E.; Oztoprak, B.G.; Kutluk, T. Comparison of novel surface treatments of al 2024 alloy for Al/CFRP adhesive bonded joints. *Int. J. Adhes. Adhes.* **2020**, *103*, 102721. [CrossRef]
11. Wang, S.Q.; Wang, Y.M.; Zou, Y.C.; Chen, G.L.; Wang, Z.; Ouyang, J.H.; Jia, D.C.; Zhou, Y. Generation, tailoring and functional applications of micro-nano pores in microarc oxidation coating: A critical review. *Surf. Eng.* **2021**, *50*, 1–22. [CrossRef]
12. Tran, Q.P.; Sun, J.K.; Kuo, Y.C.; Tseng, C.Y.; He, J.L.; Chin, T.S. Anomalous layer-thickening during micro-arc oxidation of 6061 al alloy. *J. Alloys Compd.* **2017**, *697*, 326–332. [CrossRef]
13. Wang, P.; Wei, W.X.; Pu, J.; Zhou, X.L.; Cao, W.J.; Xiao, Y.T.; Gong, Z.Y.; Hu, J. Effect of current density on characteristics of 2024 aluminum alloy micro arc oxidation coatings with titanium dioxide particles. *Int. J. Electrochem. Sci.* **2019**, *14*, 4338–4349. [CrossRef]
14. Yang, G.; Lü, X.; Bai, Y.; Cui, H.; Jin, Z. The effects of current density on the phase composition and microstructure properties of micro-arc oxidation coating. *J. Alloys Compd.* **2002**, *345*, 196–200.
15. Arunnellaiappan, T.; Kishore Babu, N.; Rama Krishna, L.; Rameshbabu, N. Influence of frequency and duty cycle on microstructure of plasma electrolytic oxidized AA7075 and the correlation to its corrosion behavior. *Surf. Coat. Technol.* **2015**, *280*, 136–147. [CrossRef]

16. Zhang, J.; Fan, Y.; Zhao, X.; Ma, R.; Du, A.; Cao, X. Influence of duty cycle on the growth behavior and wear resistance of micro-arc oxidation coatings on hot dip aluminized cast iron. *Surf. Coat. Technol.* **2018**, *337*, 141–149. [CrossRef]
17. Li, Y.; Guan, Y.; Zhang, Z.; Ynag, S. Enhanced bond strength for micro-arc oxidation coating on magnesium alloy via laser surface microstructuring. *Appl. Surf. Sci.* **2019**, *478*, 866–871. [CrossRef]
18. Wang, P.; Wu, T.; Xiao, Y.T.; Pu, J.; Guo, X.Y. Effects of $Ce(SO_4)_2$ concentration on the properties of micro-arc oxidation coatings on ZL108 aluminum alloys. *Mater. Lett.* **2016**, *182*, 27–31. [CrossRef]
19. Xin, S.G.; Song, L.X.; Zhao, R.G.; Hu, X.F. Microstructure and adhesion strength of Al-Si-O micro-arc oxidation coating. *J. Inorg. Mater.* **2006**, *21*, 493–498.
20. Egorkin, V.S.; Gnedenkov, S.V.; Sinebryukhov, S.L.; Vyaliy, I.E.; Gnedenkov, A.S.; Chizhikov, R.G. Increasing thickness and protective properties of PEO-coatings on aluminum alloy. *Surf. Coat. Technol.* **2018**, *334*, 29–42. [CrossRef]
21. Polat, A.; Makaraci, M.; Usta, M. Influence of sodium silicate concentration on structural and tribological properties of microarc oxidation coatings on 2017A aluminum alloy substrate. *J. Alloys Compd.* **2010**, *504*, 519–526. [CrossRef]
22. Li, Q.B.; Liu, C.C.; Yang, W.B.; Liang, J. Growth mechanism and adhesion of PEO coatings on 2024Al alloy. *Surf. Eng.* **2016**, *33*, 760–766. [CrossRef]
23. Gecu, R.; Yurekturk, Y.; Tekoglu, E.; Muhaffel, F.; Karaaslan, A. Improving wear resistance of 304 stainless steel reinforced AA7075 aluminum matrix composite by micro-arc oxidation. *Surf. Coat. Technol.* **2019**, *368*, 15–24. [CrossRef]
24. Zhang, K.; Yu, S. Preparation of wear and corrosion resistant micro-arc oxidation coating on 7N01 aluminum alloy. *Surf. Coat. Technol.* **2020**, *388*, 125453. [CrossRef]
25. *ASTM D4541-17*; Standard Test Method for Pull-Off Strength of Coatings Using Portable Adhesion Testers. ASTM: West Conshohocken, PA, USA, 2022.
26. Jagdheesh, R. Fabrication of a superhydrophobic Al_2O_3 Surface using picosecond laser pulses. *Langmuir* **2014**, *30*, 12067–12073. [CrossRef] [PubMed]
27. Clyne, T.W.; Troughton, S.C. A review of recent work on discharge characteristics during plasma electrolytic oxidation of various metals. *Int. Mater. Rev.* **2018**, *64*, 127–162. [CrossRef]
28. Mohedano, M.; Serdechnova, M.; Starykevich, M.; Karpushenkov, S.; Bouali, A.C.; Ferreira, M.G.S.; Zheludkevich, M.L. Active protective PEO coatings on AA2024: Role of voltage on in-situ LDH Growth. *Mater. Des.* **2017**, *120*, 36–46. [CrossRef]
29. Jiang, X.Z.; Lu, S.; Tang, L.; Wang, Z.X.; Chen, J. Influence of negative voltage on micro-arc oxidation of magnesium alloy under two steps voltage-increasing mode. *Key Eng. Mater.* **2013**, *575*, 472–476. [CrossRef]
30. Wang, S.D.; Xu, D.K.; Wang, B.J.; Sheng, L.Y.; Qiao, Y.X.; Han, E.-H.; Dong, C. Influence of phase dissolution and hydrogen absorption on the stress corrosion cracking behavior of Mg-7% Gd-5% Y-1% Nd-0.5% Zr alloy in 3.5 wt.% NaCl solution. *Corros. Sci.* **2018**, *142*, 185–200. [CrossRef]
31. Chen, X.W.; Li, M.L.; Zhang, D.F.; Cai, L.P.; Ren, P.; Hu, J.; Liao, D.D. Corrosion resistance of MoS_2-modified titanium alloy micro-arc oxidation coating. *Surf. Coat. Technol.* **2022**, *433*, 128127. [CrossRef]
32. Wang, S.D.; Xu, D.K.; Chen, X.B.; Han, E.H.; Dong, C. Effect of heat treatment on the corrosion resistance and mechanical properties of an as-forged Mg-Zn-Y-Zr alloy. *Corros. Sci.* **2015**, *92*, 228–236. [CrossRef]
33. Li, C.; Goei, R.; Li, Y.; Shi, J.; Liu, F.; Li, B.; Gao, Y.; Li, Y.; Li, S.; Tok, A.I. Effect of chromium on erosion-corrosion properties of ZrO_2-Al_2O_3 particles reinforced FE-based composites in artificial seawater slurries. *Corros. Sci.* **2022**, *198*, 110138. [CrossRef]
34. Li, J.; Ma, C.; Wang, J.; Bian, D.; Zhao, Y. Effect of pore content and pH on the corrosion behavior of hydrophobic ceramic coatings. *Int. J. Appl. Ceram. Technol.* **2022**, *20*, 1624–1635. [CrossRef]
35. Hsieh, S.F.; Ou, S.F.; Chou, C.K. The influence of the substrate on the adhesive strength of the micro-arc oxidation coating developed on TiNi shape memory alloy. *Appl. Surf. Sci.* **2017**, *392*, 581–589. [CrossRef]
36. Li, J.X.; Zhang, Y.M.; Han, Y.; Zhao, Y.M. Effects of micro-arc oxidation on bond strength of titanium to porcelain. *Surf. Coat. Technol.* **2010**, *204*, 1252–1258. [CrossRef]